Compact zooming optical systems for panoramic and telescopic applications based on curved image sensor

Do Hyeon Kim,[a] **Gil Ju Lee**,[b,*] **and Young Min Song**[a,*]
[a]Gwangju Institute of Science and Technology, School of Electrical Engineering and Computer Science, Gwangju, Republic of Korea
[b]Pusan National University, Department of Electronics Engineering, Busan, Republic of Korea

Abstract. Biological eyes in nature have strongly inspired novel optical systems. In this regard, imaging systems mimicking fish eyes and human eyes have been reported for having a wide field-of-view (FoV) and relatively higher magnification properties, respectively. However, most of these systems have complex lens configurations because of their flat image sensors. As these optical systems are bulky, heavy, and expensive, they have limited application in small devices (e.g., drones and mobile phones). In addition to a simplistic design, multi-functionality is essential for broad applications. Therefore, this study proposes a compact zooming optical system (CZOS) that combines the properties of natural vision systems (i.e., human and fish eyes) using a curved focal plane. The CZOS controls the zoom range through the modification of the distances between the single front lens (i.e., negative meniscus) and dual rear lens (i.e., bi-convex/positive meniscus lenses) groups. In the proposed system, the panoramic mode had an FoV of 200 deg and a magnification of 0.23, whereas the conversion of the system to the high magnification mode increased the magnification over two times with an FoV of 70 deg. These promising results demonstrate that the proposed simple imaging system is applicable to small-scale electronics. [DOI: 10.1117/1.JOM.2.3.031204]

Keywords: curved image sensor; wide-field-of-view; bio-inspired optics; telescopic lens; panoramic lens.

Paper 22010SS received May 19, 2022; accepted for publication Aug. 16, 2022; published online Sep. 8, 2022.

1 Introduction

Biological imaging systems of animals have developed through evolution. To promote the survival of organisms in their habitat, the imaging systems of creatures are differently optimized, e.g., for viewing angles and depth perceptions.[1–5] Consequently, because of their unique system and functionality, natural eyes have inspired the development of biomimetic cameras.[6–14] Regarding bio-inspired systems, those mimicking fish eyes have been widely studied to achieve the characteristics of a wide field-of-view (an FoV of ∼180 deg) with high visual acuity.[15–17] In addition, systems based on an imitation of human eyes, which have relatively narrower viewing angles (an FoV of ∼60 deg) than fish eyes, have been researched for the advantages of low optical aberration and high resolution.[18–20] As most conventional imaging devices employ flat image sensors, they require a multitude of lenses (7–12) to obtain high-quality visual information, thereby resulting in complex and expensive optics.[21–23] For instance, a prototype fish eye system, offering a wide FoV (∼180 deg), comprised of multi-lens optics (>6 lenses) and a flat image sensor to minimize optical aberration.[24] In addition, a reported biomimetic model of the human eye based on a flat sensor required several lenses to remove the field curvature and distortion.[25]

Meanwhile, curved image sensors have been developed to address several drawbacks of flat image sensors by deforming flexible and stretchable planes into curved forms.[26–30] Because the

*Address all correspondence to Gil Ju Lee, gjlee0414@pusan.ac.kr; Young Min Song, ymsong@gist.ac.kr

Petzval surface is a curved shape, the use of a curved image sensor facilitates a high image quality with a smaller number of lenses than a flat sensor.[31] Thus, an optical system with a curved image sensor can be closer to natural vision systems with a compact design and higher resolution than traditional imaging devices. Although recent research has yielded a complexity reduction of bio-inspired devices through the use of curved sensors,[17,20,32,33] several designs provide a limited function (i.e., fixed zoom range) because of the single-lens system. For advanced applications, such as drones and automobiles, multi-functionality of an imaging system is as essential as compactness. However, studies on bio-mimetic systems considering both compactness and functional versatility are rare.

This study proposes a compact zooming optical system (CZOS) that simultaneously reduces the complexity and provides continuous zooming modes based on curved image sensors. The CZOS can vary the zoom range continuously (70 deg to 200 deg) through the modification of the distances between the single front and dual rear lens groups, which mimics two vision systems (i.e., human and fish eyes). Further, to examine the applicability of the CZOS as the zoom lens, a simulation tool based on geometrical optics (Zemax) was used to conduct several simulations: ray-tracing, spot radius, relative illumination (RI), field curvature, angular magnification, and geometrical image analysis. The specific lens variables (e.g., thickness, radius curvature, and the distance between each lens) of the proposed optical system were optimized by utilizing constrained merit functions in the simulation tool. In addition, the red, green, and blue (RGB) light corresponding to the wavelengths of 450, 550, and 650 nm, respectively, were set as the fundamental wavelengths.

2 Results and Discussion

Figure 1(a) shows a schematic demonstrating the anatomy of the teleost eye (top) and human eye (bottom). For a wide FoV (~180 deg) with clear visual acuity in dim underwater conditions, the imaging systems of aquatic mammals include a single spherical monocentric lens and a highly light-sensitive hemispherical retina.[17] Compared with aquatic vision, the natural human eye comprises a small bi-convex lens with a small curvature, which results in a narrower FoV (~60 deg) and higher magnification. Figures 1(b) and 1(c) illustrate ray-tracing simulations for

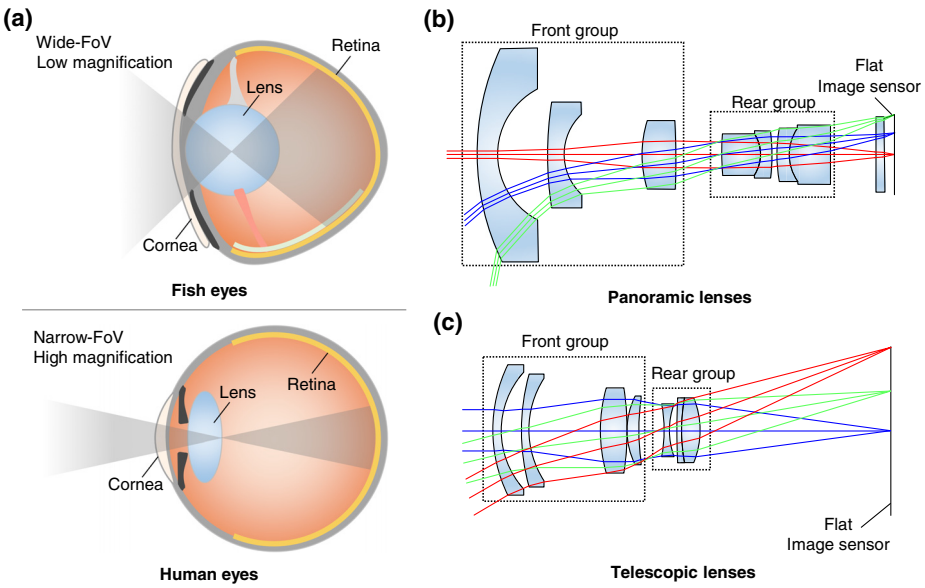

Fig. 1 (a) Schematic of a teleost eye, which is a representative fish eye for 96% of fish, (top) and a human eye (bottom) with different features of the FoV and magnification. Calculated ray-tracing results for conventional (b) panoramic and (c) telescopic optic designs using flat image surfaces. The designs of conventional systems are different from those of natural eyes because of their flat image sensors.

traditional panoramic and telescopic imaging systems based on flat image sensors. Although conventional designs have complex lens arrays, the functions of these systems are similar to those of natural eyes. The designs of both systems are provided in the Zemax software. The simulated results demonstrated the wide FoV of panoramic lenses and high magnification of telescopic lenses; however, both systems required highly complex lens configurations to flatten the field curvature onto the flat image sensor. Because large form factors of systems hinder their advanced application for devices such as drones and mobile phones, a more compact design should be fabricated by reducing the number of lenses.

The proposed CZOS, composed of three distance-adjustable lenses and a curvilinear image sensor, is shown in Fig. 2(a). Through the introduction of the curved image sensor, the complexity of an optical system can be significantly reduced compared with that of conventional biomimetic imaging systems.[29] Furthermore, the angular magnification and FoV can be varied by changing the distance between the front and rear groups (D_1). The lens configuration of the CZOS was optimized to achieve the dual-mode (i.e., panoramic and telescopic) using constrained merit functions in software. Although the variation of D_1 can provide multiple zoom modes (Fig. 5), these modes were simplified into dual modes for a simpler explanation. The specific lens variables such as thickness, material, semi-diameter, and radius of curvature (ROC) are described in Table 1. The shape of aperture is curved to avoid overlapping between lenses, as shown in Fig. 6. In the panoramic mode of the CZOS, the front and rear lenses were placed at the proper distance (D_1: 41.2 mm) to achieve a wide FoV similar to a traditional aquatic imaging system [Fig. 2(b)]. Further, compared with the conventional design, as shown in Fig. 1(b), the panoramic mode of the CZOS also offers a wide viewing angle (~200 deg) even for a small form factor (three lenses) because of the curved image sensor. When the distance between the front and rear lenses (D_1) was decreased to 5 mm, the FoV and magnification became narrower and higher, respectively, which is the telescopic mode of the CZOS [Fig. 2(c)]. As the distance variation between the front and rear groups altered the size of a light beam, the FoV and angular magnification varied with D_1. Consequently, the FoV of the telescopic mode decreased to 70 deg because of the smaller beam size. Thus, these results demonstrate that the variation of zoom range works well in a few lenses because of the curved image sensor.

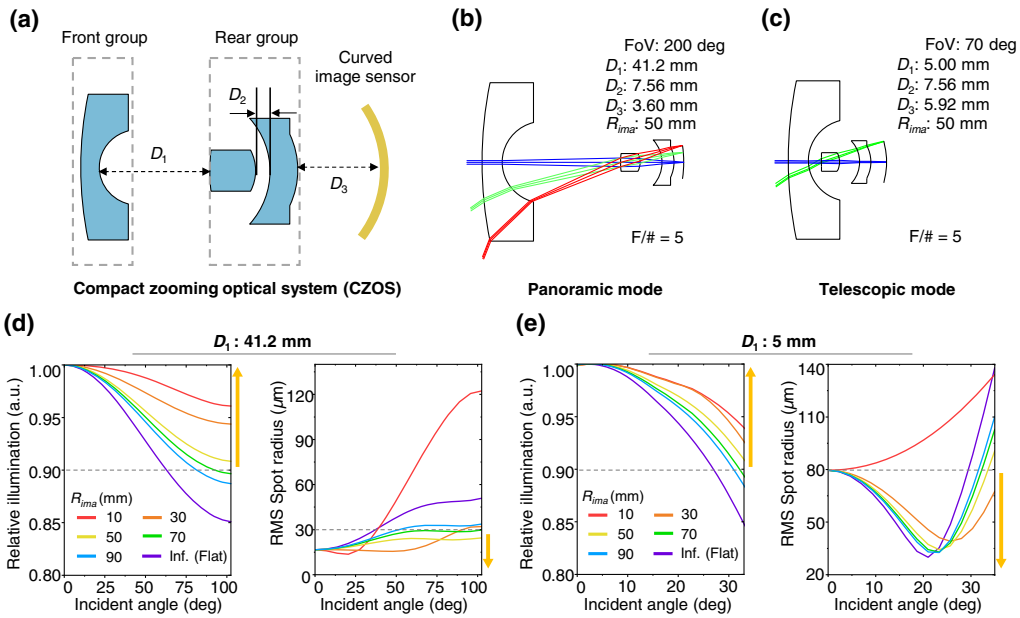

Fig. 2 (a) Schematic of proposed CZOS using a curved image sensor. Illustration of ray-tracing simulations for the CZOS in (b) panoramic and (c) telescopic modes. RI (left) and RMS spot radius (right) according to the incident angle with different ROC values of the image sensor in the (d) panoramic (D_1: 41.2 mm) and (e) telescopic (D_1: 5 mm) mode.

Table 1 Lens information of the CZOS.

Surface	Radius (mm) (first/second surface)	Thickness (mm)	Lens material	Semi-diameter (mm) (first/second surface)
Object	Infinity	Infinity	—	Infinity
1	146.05/14.67	7.00	N-BAK4	38.01/14.67
Stop	Infinity	0.20	—	1.49
2	24.90/−7.22	6.95	BK7	1.66/3.58
3	−12.10/3.60	4.21	SF10	8.20/6.31
Image	−50.00	—	—	6.93

To optimize the ROC of the image sensor (R_{ima}) in the proposed system, the effect of the shape of sensors in the system was examined [Figs. 2(d) and 2(e)]. Because the illumination and spot size are considered to be essential factors in optical systems, RI and root-mean-square (RMS) spot radius were calculated as a function of the incident angle at a wavelength of 550 nm. The evaluation of RI and RMS spot size at different wavelengths (i.e., 450 and 650 nm) are shown in Fig. 7. Because the low RI and large spot radius in an imaging system hinder obtaining high-quality images, a high value of RI and small spot size should be achieved at a wide incident angle. As shown in Fig. 2(d) (left), the illumination increased with a higher curvature (i.e., small R_{ima}) of the image sensor in the panoramic mode (D_1: 41.2 mm). Further, as the image sensor of the higher curvature approached the incident light from an object at a higher viewing angle, the RI gradually increased with the higher curvature. Thus, the highest curvature (R_{ima}: 10 mm) provided the best illumination property, whereas the flat image sensor exhibited the lowest RI. Moreover, the tendency of spot size variation differed from that of the RI as the spot radius decreased with decreasing ROC up to 50 mm and then increased up to 10 mm [Fig. 2(d); right]. This result indicates that the smallest spot size in the case of ROC is 50 mm because the shape of the focal plane is closer to the ROC of 50 mm. The ROC of 50 mm exhibited a relatively uniform and small spot radius than other shapes for wide angles. Therefore, 50 mm is the optimal ROC for achieving high-resolution imaging in the panoramic mode. In addition, the RI and spot radius size were analyzed in the telescopic mode, with the distance between the front and rear groups (D_1) being 5 mm [Fig. 2(e); left]. The illumination moderately increased with a higher curvature, similar to the panoramic mode, that is, the higher curvature sensor approached incident light at a wide angle regardless of D_1. However, the spot radius variation in the telescopic mode slightly differed from that in the panoramic mode [Fig. 2(e); right]. The results showed a similar tendency with all curvatures except for the highest (R_{ima}: 10 mm). When the distance between the image sensor and the object was reduced, the spot radius size at a large incident angle varied in a less sensitive manner with the curvature; however, an ROC of 10 mm was a sufficiently high curvature to change the spot size. As the telescopic mode of the CZOS with R_{ima}: 50 mm exhibited better performance in RI and spot radius, this was selected as the optimal ROC. In addition, these results demonstrate that a curved image sensor exhibits better performance in optical systems than a flat image sensor. The optical performance can be further improved if using a curvature variable image sensor because the optimal curvature of image sensor varies across the zoom range (Fig. 8). Further optical analyses such as distortion the modulation transfer functions (MTFs) are shown in Figs. 9 and 10, which demonstrate that the optical performance can be improved using a curved sensor (R_{ima}: 50 mm).

High resolution and uniform performance over a multi-spectral range are necessary for high-quality imaging. In particular, red, green, and blue (RGB) wavelengths have been used for estimating performance in previous research as most digital images comprise pixels that are a combination of the RGB colors.[34,35] To analyze the applicability of the proposed design as an imaging device, the RMS spot radius of CZOS was calculated at RGB wavelengths (450, 550, and 650 nm), as shown in Fig. 3(a). D_1 was set to 41.2 mm, which is the panoramic mode of CZOS, to evaluate the performance at a broad angle. For a fair comparison, the CZOS using a flat

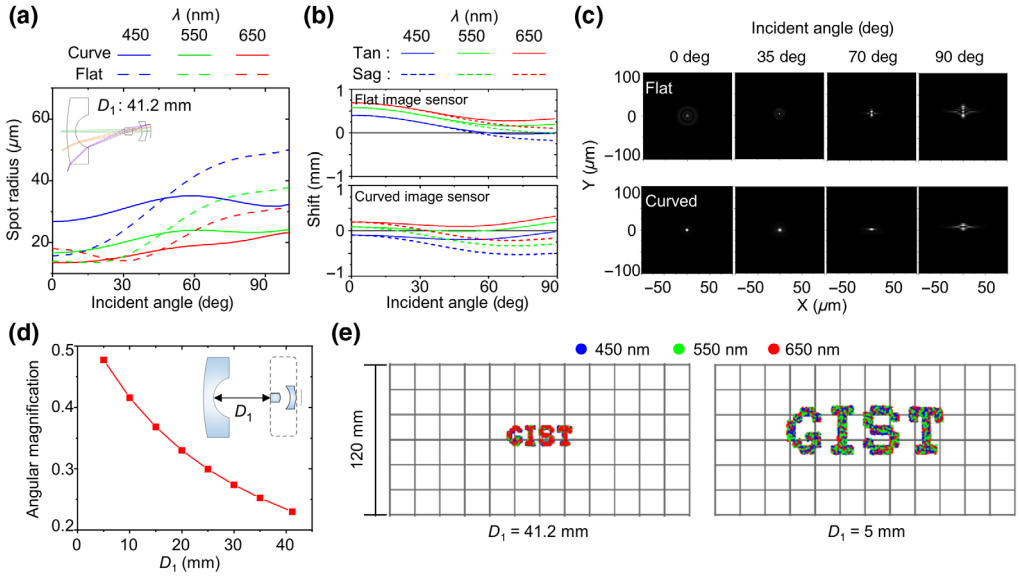

Fig. 3 (a) Spot radius for the flat image plane and curved image sensor (ROC = 50 mm) with the same lens configuration for wavelengths of 450, 550, and 650 nm. (b) Field curvature for the flat (top) and curved image (bottom) plane for red, green, and blue light (i.e., $\lambda = 450$, 550, and 650 nm, respectively). (c) Simulations of PSF according to the incident angle with different curvatures of image planes. (d) Angular magnification of CZOS with different D_1 values. (e) Simulations of geometric image analysis at the different distances between the front and rear groups (D_1).

image sensor was re-optimized (D_1: 41.2 mm, D_2: 7.1 mm, and D_3: 4.01 mm) with the same angular magnification as the CZOS based on a curved sensor. Compared with the planar sensor, the spot radius of the curved image sensor (R_{ima}: 50 mm) was similar at low incident angles (<50 deg); however, it was smaller at high incident angles (>50 deg). This result demonstrates that using the curved sensor resulted in a better and more uniform performance at a wide angle than the planar sensor even at different visible wavelengths (450, 550, and 650 nm). The spot radius diagram of the CZOS with different curvatures of the sensor is shown in Fig. 11. Further, the field curvature of CZOS at RGB wavelengths was also simulated with different shapes of the image sensors (i.e., flat and curved) [Fig. 3(b)]. For the flat image surface, the result yielded positive values at a broad incident angle [Fig. 3(b); top]. This result indicates that the focal plane was located behind the image plane at all incident angles. In contrast, the field curvature of the curved image sensor was closer to the black horizontal line at all wavelengths [Fig. 3(b); bottom], thereby indicating that the optimized curved sensor was more suitable for imaging as the focal plane of the CZOS was closer to a curved design than a flat design. Figure 3(c) shows the simulated results of the point spread function (PSF) for different sensor shapes (flat and curved) to analyze the imaging resolution. The simulated PSFs of curved sensors exhibited smaller and uniform beam sizes at a wide angle. These results demonstrate that a curved sensor facilitates a better and more uniform performance of imaging at RGB wavelengths, implying a higher image quality of CZOS because the focal plane is a curved shape. In addition, through the introduction of aspherical lenses, the optical performance (e.g., spot radius, RI, field curvature, and MTF) can be further improved (Fig. 12). The aspheric coefficients of re-optimized CZOS are given in Table 2.

Observation of distant objects requires excellent resolution and high magnification in optical systems. The above results proved that the proposed CZOS possesses a reasonable optical quality for imaging, and the magnification performance should be evaluated. Thus, to analyze the zooming ability of the CZOS, the angular magnification was calculated for varying D_1 values [Fig. 3(d)]. With decrease in the distance between the front and rear groups, the angular magnification increased because of the change in the focal length. Further, the angular magnification of the telescopic mode reached a value twice as high (0.47) as that of the panoramic mode (0.23). This result confirms the fine magnification function of the CZOS through the modification of the

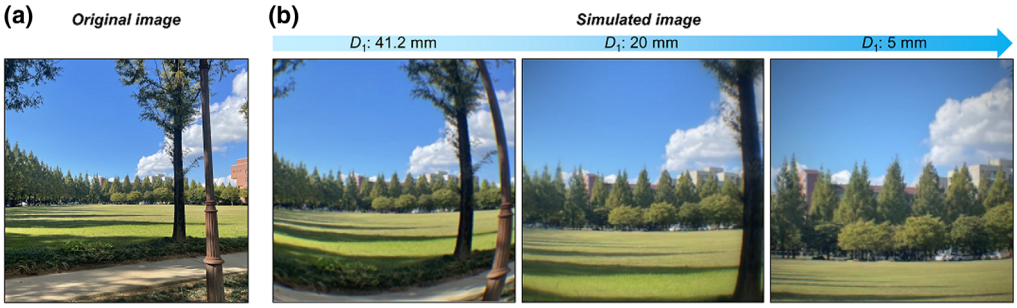

Fig. 4 (a) Object used in the imaging simulations. (b) Image simulations of an object using the CZOS with different D_1 values (41.2, 20, and 5 mm).

distance between two lens groups. Figure 3(e) shows the simulation results of the geometric image at different D_1 values (41.2 and 5 mm). A geometric image analysis was performed to confirm both the chromatic aberration and zooming properties of the CZOS. The points of the corresponding color represent the geometric images of each wavelength. The simulated image in the telescopic mode (D_1: 5 mm) yielded a bigger letter than that in the panoramic mode (D_1: 41.2 mm), thus demonstrating the magnification capability of the CZOS. In addition, the points of each wavelength were uniformly arranged as the CZOS exhibited good performance in the spot radius and field curvature analysis. Thus, these results demonstrate the zooming function of the CZOS and low chromatic aberration in both panoramic and telescopic modes.

Figure 4 shows the results of an image simulation for an object with varying distances between the front and rear groups. In this process, the sizes of the systems were adjusted to obtain an effective focal length (EFL) of 6.2 mm, and the F-number of 5 was used. Further, the object height was set by D_1 to correspond to each FoV. Compared with the original image [Fig. 4(a)], the simulated image in the panoramic mode (D_1: 41.2 mm) exhibited a wide FoV, which almost fully yielded the original image [Fig. 4(b); left]. The middle of Fig. 4(b) shows the magnified image at 20 mm of D_1, which shows a narrower FoV than the panoramic mode. However, a much-magnified image was obtained when the front and rear groups approached 5 mm [Fig. 4(b); right]. These results practically demonstrate the simple and continuous magnification method of the CZOS and high image quality of a curved focal plane. In addition, the lenses of the CZOS can be replaced with a plastic material, as the performance of the plastic-based system (p-CZOS) is similar to the CZOS (Fig. 13, Table 3). These results demonstrate the universality of our system.

3 Conclusions

This study investigated the applicability of the CZOS with curved image sensors as a continuous zooming system through ray-tracing simulations. Optical analysis factors, such as the RI and spot radius size, provided a design rule for the optimum ROC of the image sensor (i.e., 50 mm). The calculated results indicated that the curved image sensor reduced the complexity of the CZOS while maintaining low optical aberration. In addition, the simulation results of field curvature and spot radius at different wavelengths (450, 550, and 650 nm) demonstrated that the CZOS yielded a low chromatic aberration and consistent optical performance at a wide viewing angle. Finally, the image analysis demonstrated the high imaging performance of the CZOS in the variation of the FoV (70 deg to 200 deg). These results indicate that the proposed imaging system exhibits a reasonable optical quality for imaging and magnification function. The simple imaging system is expected to be applicable to compact devices such as drones and automobiles.

4 Appendix

We expect that the data in the appendices will benefit the reader's understanding of the work.

Figure 5 presents the continuous zooming property (70 deg to 200 deg) of the CZOS.

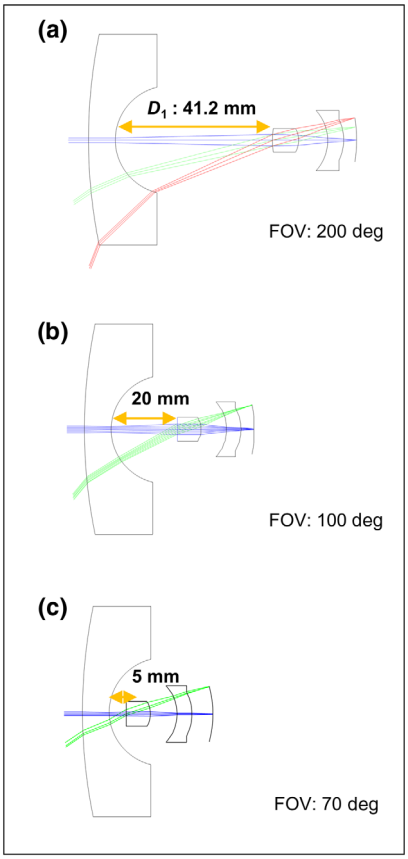

Fig. 5 Illustration of ray-tracing simulations for CZOS with different D_1 values of (a) 41.2 mm, (b) 20 mm, and (c) 5 mm. The variation of distance changes the FoV of the system.

Figure 6 presents the shape of aperture in CZOS to avoid the overlapping between lens.

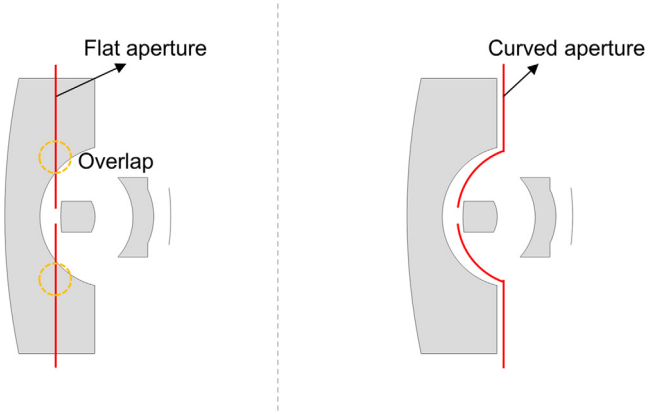

Fig. 6 Schemes of lens configurations with a flat aperture (left) and a curve aperture (right).

Figure 7 presents the evaluation of RI and RMS spot size at different wavelengths (i.e., 450, 650 nm).

Figure 8 presents the RI and spot radius with different ROC. This result indicates that the optical performance can be further improved if using a curvature variable sensor.

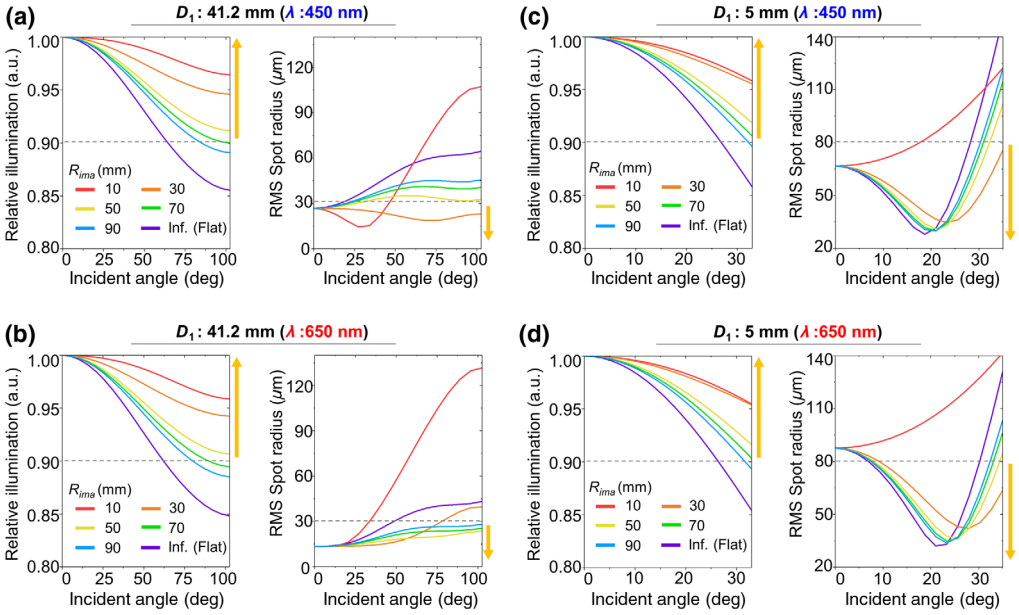

Fig. 7 RI and RMS spot radius according to the incident angle with different ROC values of the image sensor in panoramic (D_1: 41.2 mm) at wavelengths of (a) 450 nm and (b) 650 nm and in telescopic (D_1: 5 mm) mode at wavelengths of (c) 450 nm and (d) 650 nm.

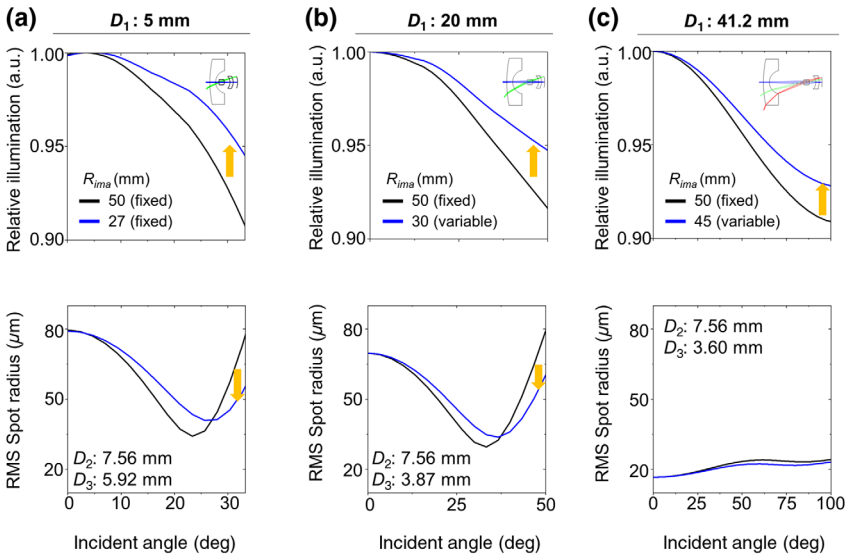

Fig. 8 RI (top) and RMS spot radius (bottom) according to the incident angle with different ROC values of image sensor when D_1: (a) 5; (b) 20; and (c) 41.2 mm.

Figure 9 shows the MTFs of CZOS with different incident angles and D_1.

Figure 10 shows the distortion characteristic of CZOS.

Figure 11 shows the spot diagram of the systems using flat and curved image sensors.

Figure 12 presents the comparison of optical performances between spherical lens system and aspherical lens system. Through the introduction of aspherical lenses, the optical performance (e.g., spot radius, relative illumination, field curvature, and MTF) can be further improved.

Table 2 shows the used aspheric coefficient in Fig. 12.

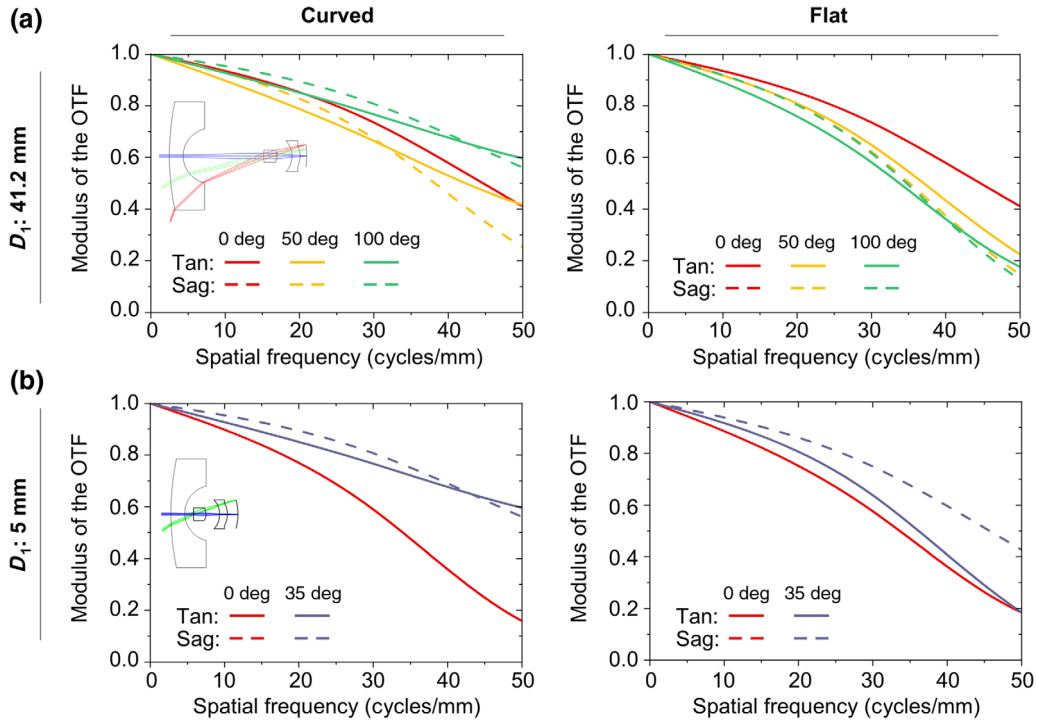

Fig. 9 MTFs of CZOS with different incident angles when D_1: (a) 41.2 mm and (b) 5 mm at wavelengths of 450 to 650 nm.

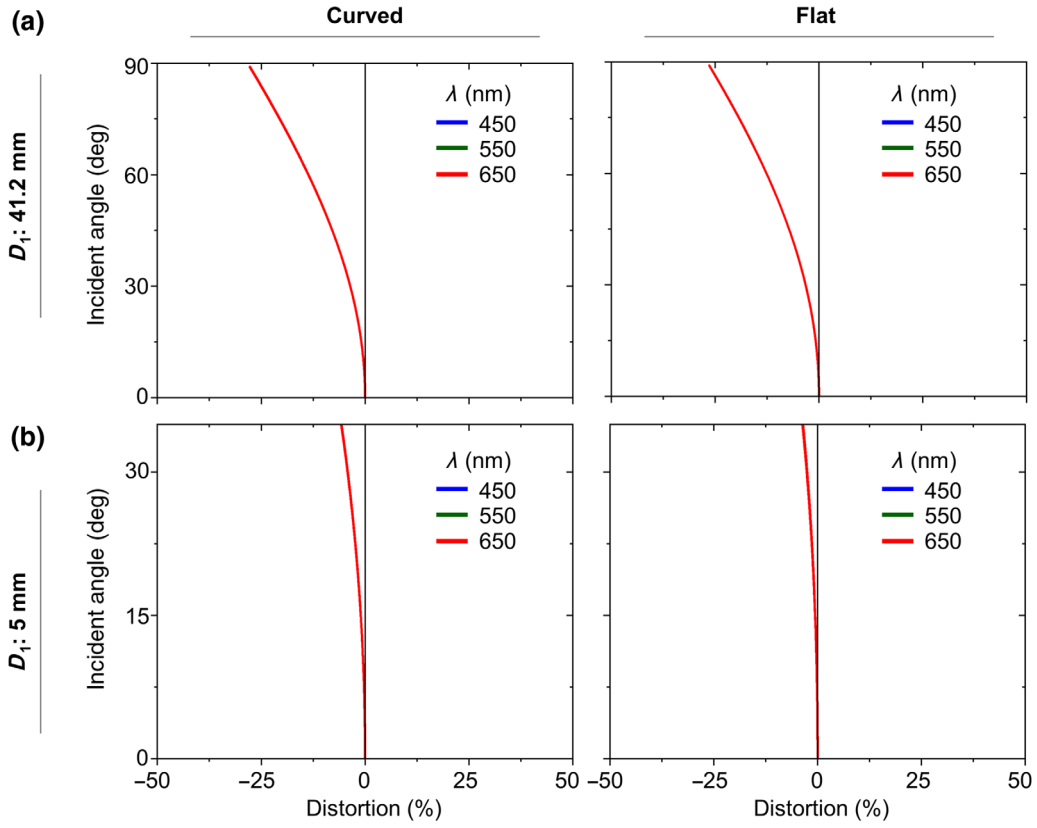

Fig. 10 F-theta distortion with different incident angles when D_1: (a) 41.2 mm and (b) 5 mm at wavelengths of 450, 550, and 650 nm.

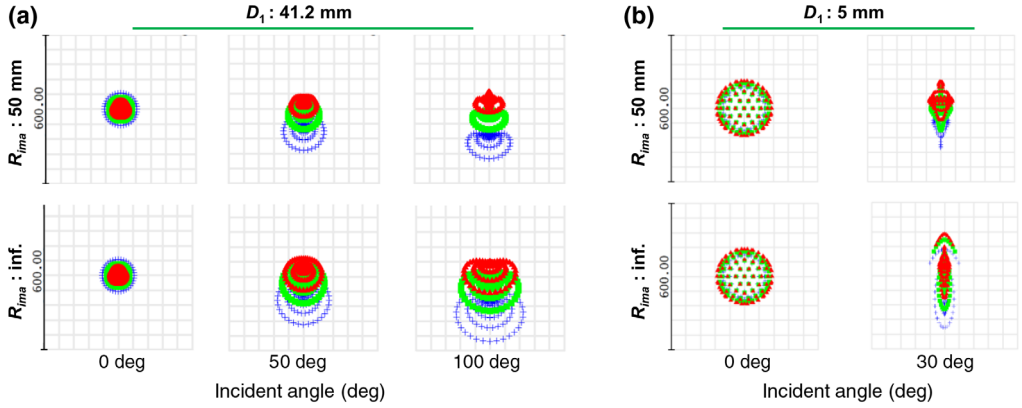

Fig. 11 Calculated spot radius diagram when (a) panoramic mode and (b) telescope mode with different ROC values. The scale bar is 600 μm.

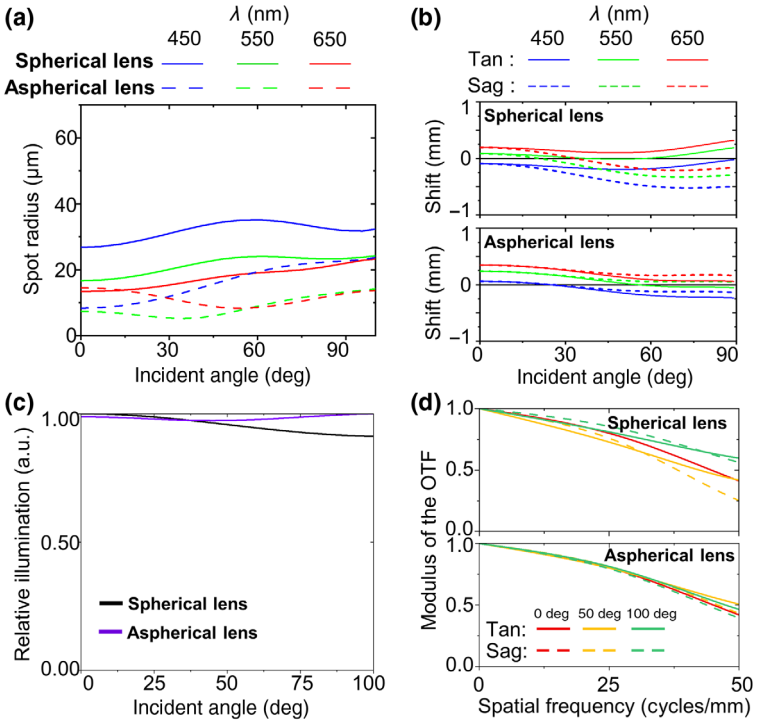

Fig. 12 Spot radius for the CZOS utilizing spherical lenses and aspherical lenses for wavelengths of 450, 550, and 650 nm. (b) Field curvature for the system based on spherical lens (top) and aspherical lens (bottom) for red, green, and blue light (i.e., $\lambda = 450$, 550, and 650 nm, respectively). (c) RI according to the incident angle and (d) MTFs of both systems.

Table 2 Aspheric coefficients for the re-optimized CZOS utilizing the aspherical lenses.

Surface	Conic constant	2nd	4th	6th	8th	10th	12th	14th	16th
1	0	0	0	0	0	0	0	0	0
	0	0	0	0	0	0	0	0	0
2	0	0	–5.3*E*–04	0	0	0	0	0	0
	0	0	7.1*E*–04	1.7*E*–07	0	0	0	0	0
3	0	0	0	0	0	0	0	0	0
	0	0	–8.7*E*–07	–9.7*E*–07	0	0	0	0	0

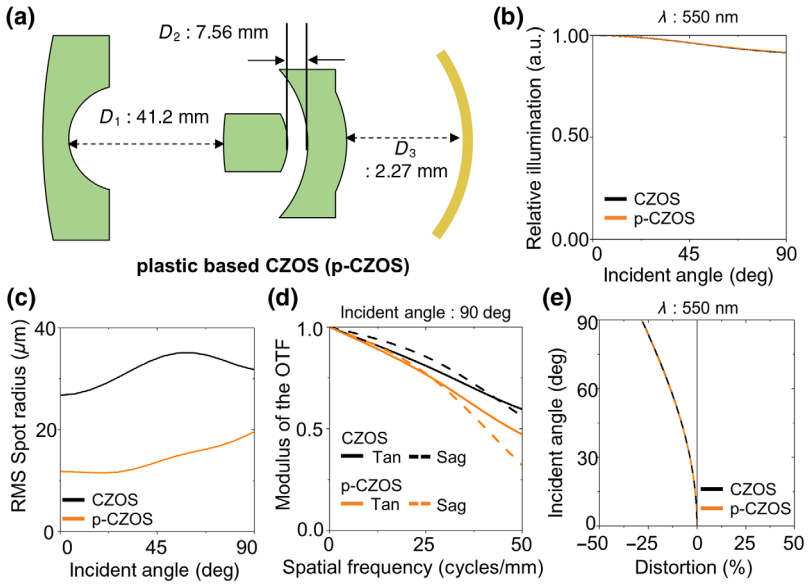

Fig. 13 (a) Schematic of revised CZOS utilizing plastic lenses (p-CZOS). (b) RI and (c) RMS spot radius according to the incident angle with different lens systems (CZOS, p-CZOS). (d) MTFs and (e) *F*-theta distortion of both systems.

Figure 13 presents the comparison of optical performances between CZOS and plastic based CZOS. The lenses of the CZOS can be replaced with a plastic material, as the performance of plastic based system (p-CZOS) is similar to the CZOS.

Table 3 shows the plastic lens information of the system in Fig. 13.

Table 3 Lens information of the revised CZOS utilizing plastic lenses.

Surface	Radius (mm) (first/second surface)	Thickness (mm)	Lens material	Semi-diameter (mm) (first/second surface)
Object	Infinity	Infinity	—	Infinity
1	146.05/14.67	7.00	APL5014CL	38.01/14.67
Stop	Infinity	0.20	—	1.40
2	24.90/−7.22	6.95	APL5014CL	1.66/3.58
3	−12.10/−13.50	4.21	OKP-A2	8.20/6.31
Image	−50.00	—	—	6.79

Acknowledgments

This research was supported by the GIST Research Institute (GRI) through a grant funded by the GIST and National Research Foundation of Korea (Grant No. NRF2017M3D1A1039288, NRF2021R1A4A2001827). This work was also supported by the Institute of Information & Communications Technology Planning & Evaluation (IITP) through a grant funded by the Korean government (MSIT) (Grant No. 2020-0-01000, Light field and LiDAR sensor fusion systems for full self-driving). The authors declare that they have no conflicts of interest.

Code, Data, and Materials Availability

No data were generated or analyzed in the presented research.

References

1. T. Nagata et al., "Depth perception from image defocus in a jumping spider," *Science* **335**, 469–471 (2012).
2. M. F. Land and R. D. Fernald, "The evolution of eyes," *Annu. Rev. Neurosci.* **15**, 1–29 (1992).
3. S. Yamashita and H. Tateda, "Spectral sensitivities of jumping spider eyes," *J. Comp. Physiol.* **105**, 29–41 (1976).
4. M. F. Land, "The optics of animal eyes," *Contemp. Phys.* **29**, 435–455 (1988).
5. W. Jagger and P. Sands, "A wide-angle gradient index optical model of the crystalline lens and eye of the rainbow trout," *Vis. Res.* **36**, 2623–2639 (1996).
6. Y. M. Song et al., "Digital cameras with designs inspired by the arthropod eye," *Nature* **497**, 95–99 (2013).
7. Q. Guo et al., "Compact single-shot metalens depth sensors inspired by eyes of jumping spiders," *Proc. Natl. Acad. Sci.* **116**, 22959–22965 (2019).
8. F. Zhou et al., "Optoelectronic resistive random access memory for neuromorphic vision sensors," *Nat. Nanotechnol.* **14**, 776–782 (2019).
9. W. Lee et al., "Two-dimensional materials in functional three-dimensional architectures with applications in photodetection and imaging," *Nat. Commun.* **9**, 1417 (2018).
10. W. L. Tsai et al., "Band tunable microcavity perovskite artificial human photoreceptors," *Adv. Mater.* **31**, 1900231 (2019).
11. K. Kim et al., "Biologically inspired ultrathin arrayed camera for high-contrast and high-resolution imaging," *Light-Sci. Appl.* **9**, 28 (2020).
12. D. Floreano et al., "Miniature curved artificial compound eyes," *Proc. Natl. Acad. Sci.* **110**, 9267–9272 (2013).
13. T. Chung et al., "Mining the smartness of insect ultrastructures for advanced imaging and illumination," *Adv. Funct. Mater.* **28**, 1705912 (2018).
14. H. K. Raut et al., "Multiscale ommatidial arrays with broadband and omnidirectional anti-reflection and antifogging properties by sacrificial layer mediated nanoimprinting," *ACS Nano* **9**, 1305–1314 (2015).
15. G. J. Lee, W. I. Nam, and Y.M. Song, "Robustness of an artificially tailored fisheye imaging system with a curvilinear image surface," *Opt. Laser Technol.* **96**, 50–57 (2017).
16. Y. Xiong and K. Turkowski, "Creating image-based VR using a self-calibrating fisheye lens," in *Proc. IEEE Comput. Soc. Conf. Comput. Vis. And Pattern Recognit.*, IEEE, San Juan, pp. 237–243 (1997).
17. M. S. Kim et al., "An aquatic-vision-inspired camera based on a monocentric lens and a silicon nanorod photodiode array," *Nat. Electron.* **3**, 546–553 (2020).
18. H. C. Ko et al., "A hemispherical electronic eye camera based on compressible silicon opto-electronics," *Nature* **454**, 748–753 (2008).
19. Z. Rao et al., "Curvy, shape-adaptive imagers based on printed optoelectronic pixels with a kirigami design," *Nat. Electron.* **4**, 513–521 (2021).
20. C. Choi et al., "Human eye-inspired soft optoelectronic device using high-density MoS2-graphene curved image sensor array," *Nat. Commun.* **8**, 1664 (2017).
21. L. Fan and L. Lu, "Design of a simple fisheye lens," *Appl. Opt.* **58**, 5311–5319 (2019).
22. Y. Yan and J. Sasian, "Photographic zoom fisheye lens design for DSLR cameras," *Opt. Eng.* **56**, 095103 (2017).
23. G. Ming, C. Yang, and Z. Xibin, "Optical system design of four-channel dual-band infrared panoramic imaging," *Opt. Eng.* **58**(4), 045104 (2019).
24. H. Choi, J. Ryu, and J. Kim, "A novel fisheye-lens-based photoacoustic system," *Sensors* **16**, 2185 (2016).
25. S. Regal et al., "Biomimetic models of the human eye, and their applications," *Nanotechnology* **32**, 302001 (2021).
26. D. Dumas et al., "Infrared camera based on a curved retina," *Opt. Lett.* **37**, 653–655 (2012).
27. B. Guenter et al., "Highly curved image sensors: a practical approach for improved optical performance," *Opt. Express* **25**, 13010–13023 (2017).
28. Y. Xuan et al., "Active-matrix-based flexible optical image sensor," *Adv. Mater. Technol.* **6**, 2100259 (2021).

29. H. Saito et al., "Compound eye shaped flexible organic image sensor with a tunable visual field," in *18th IEEE Int. Conf. Micro Electro Mech. Syst.*, IEEE, Miami Beach, pp. 96–99 (2005).
30. B. Chambion et al., "Tunable curvature of large visible CMOS image sensors: Towards new optical functions and system miniaturization," in *IEEE 66th Electron. Comp. and Technol. Conf. (ECTC)*, IEEE, Las Vegas, pp. 178–187 (2016).
31. W. Gao et al., "Recent advances in curved image sensor arrays for bioinspired vision system," *Nano Today* **42**, 101366 (2022).
32. K. Zhang et al., "Origami silicon optoelectronics for hemispherical electronic eye systems," *Nat. Commun.* **8**, 1782 (2017).
33. H. S. Son et al., "Design of a spherical focal surface using close-packed relay optics," *Opt. Express*, **19**, 16132–16138 (2011).
34. P. Wang, N. Mohammad, and R. Menon, "Chromatic-aberration-corrected diffractive lenses for ultra-broadband focusing," *Sci. Rep.* **6**, 21545 (2016).
35. L. Prey, M. von Bloh, and U. Schmidhalter, "Evaluating RGB imaging and multispectral active and hyperspectral passive sensing for assessing early plant vigor in winter wheat," *Sensors* **18**, 2931 (2018).

Do Hyeon Kim received his BS degree from the School of Electrical Engineering and Computer Science (EECS), Gwangju Institute of Science and Technology (GIST), Gwangju, Korea, in 2019. He is currently an integrated PhD student at Gwangju Institute of Science and Technology (GIST).

Gil Ju Lee received his BS degree from the Department of Electronics Engineering, Pusan National University, Busan, Korea, in 2016. He obtained his integrated MS/PhD degree from the School of Electrical Engineering and Computer Science (EECS), Gwangju Institute of Science and Technology (GIST), Gwangju, Korea, in 2021. He is currently an associate professor at Pusan National University, Korea.

Young Min Song received his BS degree from the Department of Biomedical Engineering, Yonsei University, Korea, in 2004. He obtained his MS degree from the Department of Information and Communications, Gwangju Institute of Science and Technology (GIST), Gwangju, Korea, in 2006. He received his PhD from the School of Information and Mechatronics, GIST in 2011. He is currently a professor at Gwangju Institute of Science and Technology, Korea.